Janus Micelles

ARTICLE *in* MACROMOLECULES · FEBRUARY 2001

Impact Factor: 5.8 · DOI: 10.1021/ma000670p · Source: OAI

Janus Micelles†

Rainer Erhardt,‡ Alexander Böker,‡,§ Heiko Zettl,§ Håkon Kaya,|| Wim Pyckhout-Hintzen,|| Georg Krausch,§,⊥ Volker Abetz,*,‡ and Axel H. E. Müller*,‡,⊥

Makromolekulare Chemie II, Universität Bayreuth, D-95440 Bayreuth, Germany; Physikalische Chemie II, Universität Bayreuth, D-95440 Bayreuth, Germany; Institut für Festkörperforschung, Forschungszentrum Jülich, D-52425 Jülich, Germany; and Bayreuther Zentrum für Kolloide und Grenzflächen, D-95440 Bayreuth, Germany

Received April 19, 2000; Revised Manuscript Received October 30, 2000

ABSTRACT: A novel strategy to synthesize amphiphilic surface-compartmentalized nanoparticles based on linear ABC triblock copolymers is presented. These so-called Janus micelles consist of a cross-linked core and a corona with a "northern" and a "southern" hemisphere. Selectively cross-linking spherical domains of the polybutadiene middle block in a well-ordered bulk morphology of a polystyrene-*block*-polybutadiene-*block*-poly(methyl methacrylate) triblock copolymer (SBM) leads to the conservation of the compartmentalization of the outer blocks after dissolution of the material. Multi-angle laser light scattering gel permeation chromatography, fluorescence correlation spectroscopy, small-angle neutron scattering, and static and dynamic light scattering, as well as scanning force microscopy, indicate the existence of an equilibrium between molecularly dissolved Janus micelles (unimers) and aggregates (multimers), so-called supermicelles.

Introduction

During the past few years a variety of novel bulk morphologies has been established for linear binary[1−3] and ternary block copolymers[2,4−7] as well as for block copolymers with nonlinear chain topologies.[8−11] The amphiphilic nature of block copolymers composed of incompatible blocks has long been recognized, and a large number of studies have addressed the solution behavior of binary[12−16] and, more recently, ternary block copolymers.[17−20] In most of these investigations block copolymers were allowed to self-assemble or to dissolve on a molecular level in various solvents. Selective solvents often lead to the formation of micelles, where the less soluble parts of the block copolymers form core domains which are surrounded by a highly swollen corona of the more soluble blocks. Depending on the degree of swelling of the corona and the relative composition of the block copolymers, various shapes of micelles have been found, which in general show spherical or cylindrical symmetries. To our knowledge Liu and co-workers were the first who selectively cross-linked one component in block copolymers in order to obtain larger structures like spheres[19] or cylinders.[21] The term "Janus" used to describe the property of having two faces (a hydrophobic and a hydrophilic one) was first used in natural science by Veyssié et al. who created "Janus beads" by a partial hydrophobic modification of commercial glass spheres.[22,23] Schlüter and co-workers reported on rodlike molecules with two different half-coronas based on polydendrons.[24] Further cylindrical Janus-type structures were obtained by sequential ring-opening metathesis polymerization of polystyrene and poly(ethylene oxide) macromonomers.[25]

However, noncentrosymmetric structures taking advantage of the inherently noncentrosymmetric nature of ABC triblock copolymers have not been reported on so far. While noncentrosymmetric lamellae were found in self-assembled blends of linear ABC triblock copolymers with AC[26] or other ABC block copolymers,[27] pure block copolymers typically form centrosymmetric structures in the bulk state. In the present contribution, the synthesis and characterization of noncentrosymmetric particles, so-called "Janus micelles", will be reported. Following an idea of Reimund Stadler, the particles are obtained via a three-step procedure (see Figure 1): (i) a film of an ABC triblock copolymer with lamellae of the outer blocks embedding spherical domains of the middle block (the so-called *lamellae−sphere* or *ls*-morphology)[5] is prepared by solution casting, (ii) the spherical domains of the middle blocks are cross-linked in the bulk state, and (iii) the bulk phase is redissolved in a good solvent.

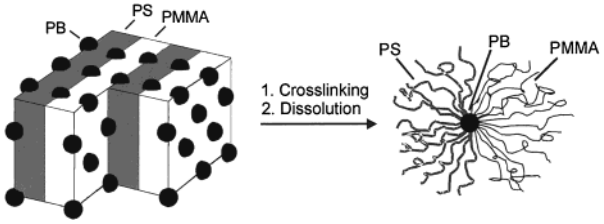

Figure 1. Schematic representation of the Janus micelles' synthesis (left-hand side: sketch of SBM ls-morphology).

Experimental Section

Synthesis. SBM Precursor. The Janus micelles' precursor, a polystyrene-*block*-polybutadiene-*block*-poly(methyl methacrylate) (SBM) triblock copolymer, was synthesized via sequential anionic polymerization in tetrahydrofuran (THF), following procedures described elsewhere.[28]

Cross-Linking. The bulk cross-linking was performed in two ways. In the first approach, a film of SBM cast from chloroform ($CHCl_3$) solution was swollen in acetonitrile for 48 h (without destroying the morphology) and afterward cross-linked by adding 5% (v/v) disulfurdichloride (S_2Cl_2) and waiting for another 48 h.[29−31] The product was purified in the following

† Dedicated to the memory of Prof. Dr. Reimund Stadler
‡ Makromolekulare Chemie II, Universität Bayreuth.
§ Physikalische Chemie II, Universität Bayreuth.
|| Forschungszentrum Jülich.
⊥ Bayreuther Zentrum für Kolloide und Grenzflächen.

10.1021/ma000670p CCC: $20.00
Published on Web 01/17/2001

way: The film was rinsed three times with acetonitrile and dried in a vacuum. Afterward it was redissolved in THF and reprecipitated in methanol twice and dried in a vacuum at room temperature. In the second approach a solution cast film of SBM containing 5% (w/w) α,α′-azoisobutyronitrile (AIBN) was annealed at 90 °C for 48 h in a vacuum for the radical cross-linking process. This product was also purified by redissolution and reprecipitation and dried in a vacuum.

Transmission Electron Microscopy (TEM). The bulk morphology of the SBM block copolymer was examined using TEM. Films (around 1 mm thick) were cast from 10% (w/w) solutions in $CHCl_3$ and allowed to evaporate slowly for 2 weeks. The as-cast films were dried for 1 day in a vacuum at room temperature. Thin sections were cut at room temperature using a Reichert-Jung Ultracut E microtome equipped with a diamond knife. To enhance the electron density contrast between the three blocks, the sections were exposed to OsO_4 vapor for 60 s, which leads to a preferential staining of the polybutadiene block (appears black). Bright field TEM was performed using a Zeiss CEM 902 electron microscope operated at 80 kV.

Multi-Angle Laser Light Scattering Gel Permeation Chromatography (MALLS−GPC). MALLS−GPC measurements were performed at room temperature using a GPC equipped with a Wyatt Technology DAWN DSP−F detector (Ar ion laser, $\lambda_0 = 488$ nm) and a Shodex-RI-71 detector. Further experimental conditions were tailored for the respective polymer. In the measurements of the SBM, three 30 cm 5 μm PSS SDV columns were used (10^3, 10^5, and 10^6 Å) with THF as eluent at a flow rate of 1 mL/min ($c \approx 2$ g/L; injection volume = 100 μL). In the case of the cross-linked SBMs one 30 cm 10 μm PSS SDV LINEAR ONE column was used with THF containing 0.25% tetrabutylammonium bromide as eluent at a flow rate of 0.25 mL/min ($c = 0.2-0.4$ g/L; injection volume = 50 μL). The salt was added to the solvent in order to prevent polymer adsorption on the columns.

Asymmetric Flow Field-Flow Fractionation (FFFF).[32,33] The measurement was done on a Postnova Analytics HRFFF-10000 system equipped with RI and UV detectors and a PD2000 light scattering detector with THF as eluent. The following experimental conditions were applied: polymer concentration ≈ 1 g/L; spacer thickness = 0.35 mm; membrane cutoff molecular weight = 5000; injection volume = 20 μL; measuring time = 20 min; cross-flow gradient = 80% − 0%, parabolic within 20 min; laminar flow out = 0.5 mL/min within 20 min; laminar flow in = 2.5−0.5 mL/min within 22 min; injection time = 60 s; focusing time = 60 s.

Confocal Fluorescence Correlation Spectroscopy (FCS). The FCS experiments were carried out using a Zeiss ConfoCor 2 spectrometer. This instrument consists of an Axiovert microscope with a coverslip corrected 40× water immersion objective, a He−Ne laser, and a variable pinhole. For detection, an avalanche photodiode (APD) in single photon counting mode was used. This experimental setup allows FCS studies with confocal optics. Further details of FCS have already been described earlier.[34,35] The setup is commonly used for measurements in water. Slight modifications were necessary to enable measurements in organic solvents. Rhodamin B (Lambdachrome, $\lambda_{exc} = 552$ nm, $\lambda_{emiss} = 580$ nm) was chosen as dye. For excitation, the 543 nm line of the He−Ne laser was used in combination with a pinhole diameter of 78 μm. The solubility of the polar Rodamin B dye in THF is low (on the order of 10^{-5} mol/L). In the presence of Janus micelles, part of the dye molecules are expected to be located within the Janus micelles due to favorable interaction. A fit of the autocorrelation function as a two-particle problem results in the diffusion time of the free Rhodamin B and the diffusion time of the micelles labeled with Rhodamin B. The diffusion coefficents and the hydrodynamic radii were calculated based on the beam waist radius determined from measurements of Rhodamin 6G in water (no data for Rhodamin 6G in THF available). The waist radius difference between water and THF is expected to be negligible due to the small refractive index difference between the two solvents. FCS measurements were performed for polymer concentrations ranging from 0.515 × 10^{-4} to 1 g/L. A constant Rhodamin B concentration of 1 × 10^{-11} mol/L was used.

Small-Angle Neutron Scattering (SANS). Setup. The SANS experiments were carried out on the instrument KWS1 at the DIDO research reactor at the Forschungszentrum Jülich. The measurements were performed at three detector/collimation distances, viz. 20 m/20 m, 8 m/8 m, and 2 m/4 m. The chosen wavelength was 7 Å, thus giving a q range of 0.002 Å$^{-1} \le q \le 0.2$ Å^{-1}.

Calibration Measurements. Raw Data Corrections. The raw data contain intensity contributions from the solvent, the empty cell, coherent sample scattering, and the electronic background. The latter contribution was measured by blocking the beam with a boron carbide slab, and the result was subtracted from all other measurements. The background intensity I_{bg} and the scattering intensity produced by the sample cell I_{cell} were removed according to

$$I(q) = (I_{sample} - I_{bg}) - \left(\frac{T_{sample}}{T_{ec}}\right)(I_{cell} - I_{bg}) \qquad (1)$$

where I is the number of detector counts normalized to the incoming number of neutrons. The subscript bg denotes the electronic background. T_{sample} and T_{ec} are the transmissions of the sample and the empty cell, respectively.

The absolute scattering cross section of the sample was obtained with a flat scattering Lupolen standard (superscript S refers to the standard):

$$\frac{d\Sigma}{d\Omega}(q) = \frac{D^S T^S}{DT}\left(\frac{L^S}{L}\right)^2 \frac{I(q)}{I^S(0)}\left(\frac{d\Sigma}{d\Omega}(q)\right)^S \qquad (2)$$

D, T, and L are the sample thickness, transmission, and sample-to-detector distance, respectively. $I^S(0)$ is the mean scattering level from the standard. The value $(d\Sigma/d\Omega(q))^S$ is known through calibration with vanadium. The data are corrected for incoherent solvent scattering by a proper weighting within the same function.

The Unified Exponential/Power Law Equation. Starting with general expressions for the classical Porod correlation function $\gamma(r)$, Beaucage developed a universal equation which describes the entire scattering curve for a multitude of complex systems consisting of randomly distributed structures, or structures comprising several substructures.[36] The equation is a combination of approximations, viz. Guinier-like exponentials and generalized power laws, each describing different structural levels. These approximations are limited to the structural levels in which they are valid regarding size and morphology of the relevant structure. Transitions from one structural level to another is taken into account by error-function terms and exponential cutoffs.

$$\frac{d\Sigma}{\Phi d\Omega}(q) \approx G\exp\left(\frac{-q^2 R_g{}^2}{3}\right) + B\exp\left(\frac{-q^2 R_{sub}{}^2}{3}\right)\left[\frac{(\mathrm{erf}(qR_g/\sqrt{6}))^3}{q}\right]^P + G_s\exp\left(\frac{-q^2 R_s{}^2}{3}\right) + B_s\left[\frac{(\mathrm{erf}(qR_s/\sqrt{6}))^3}{q}\right]^{P_s} \qquad (3)$$

Equation 3 describes the scattering from a superstructure with overall radius of gyration R_g, consisting of smaller-scale structures of size R_s. G is the Guinier prefactor, and B is the prefactor of the power law with exponent P. The power law has a cutoff at R_{sub}, which in general is equal to R_s. G_s and B_s are the prefactors of the Guinier/power law behavior occurring at the smaller structural level, and P_s is the subscale power law coefficient. As eq 3 is constructed from asymptotic scattering laws, it cannot be applied to monodisperse, well-defined structures, which yield scattering curves showing oscillations.

Note that we are fitting the Beaucage model to the macroscopic scattering cross section normalized by concentration, with the intention to realize a simultaneous fit of the scattering

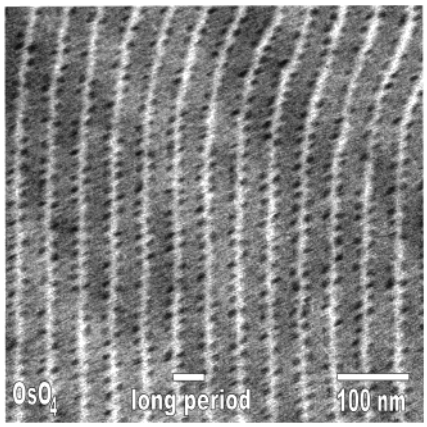

Figure 2. TEM micrograph of $S_{51}B_6M_{43}^{190}$ stained with OsO_4 (ls-morphology). The lamellae of PS and PMMA appear gray and light, while the PB spheres are dark.

curves obtained at different concentrations. This will only affect the prefactors in eq 3. From the shape of the scattering curves, it can be inferred that the scattering particles retain the same structure in the measured concentration range 0.025−3 g/L.

Light Scattering. Static light scattering experiments (SLS) were carried out on a SLS goniometer 1 (Sofica) using a He−Ne laser ($\lambda_0 = 632.8$ nm). The refractive index increment dn/dc, which is needed for the evaluation of the SLS data, was measured with a scanning Michaelson interferometer.[37] Dynamic light scattering (DLS) was performed on an ALV-SP 52 goniometer using an ALV 5000 correlator and a Kr ion laser ($\lambda_0 = 647.1$ nm). Prior to the light scattering experiments the Janus micelle solutions were filtered using Millipore filters (housing: polypropylene, membrane: poly(tetrafluoroethylene)) with a pore size of 3 μm (filters with smaller pore sizes were rapidly clogged).

Scanning Force Microscopy. The scanning force microscopy (SFM) images were taken on a Digital Instruments Dimension 3100 microscope operated in Tapping Mode (free amplitude of the cantilever ≈ 20 nm; set point ratio ≈ 0.98). The standard silicon nitride cantilevers were driven at a frequency about 3% below resonance. Height and phase images were recorded at scanning velocities of around 6 μm/s. Phase images can reveal lateral variations in the local elasticity (bright areas correspond to larger phase shifts than darker regions). For a correct evaluation of the mean radii of the micelles, one has to correct for the finite radius of curvature of the tip, which systematically enlarges the lateral dimensions of elevated objects. In this study tips were changed regularly in order to avoid contamination. We assume that all tips had a radius of curvature of about $t = 10$ nm, which was subtracted from the measured radii.

Results and Discussion

Synthesis. The starting material for the synthesis of the Janus micelles is a SBM triblock copolymer of the composition $S_{51}B_6M_{43}^{190}$. The subscript numbers denote the mass fraction in percent and the superscript gives the number-average molecular weight M_n in kg/mol (M_n was calculated using the M_n of the PS precursor[38] determined by GPC and the composition of the triblock copolymer determined by ^{1}H NMR). In the bulk, this polymer exhibits the so-called ls-morphology[5] with very narrowly distributed polybutadiene (PB) spheres located at the interface of the polystyrene (PS) and poly(methyl methacrylate) (PMMA) lamellae as shown in Figure 2 and schematically on the left-hand side of Figure 1. Please note that the PS/PMMA ratio (as determined by ^{1}H NMR) is not reflected in the apparent volume fractions visible in the TEM image due to partial degradation of PMMA in the electron beam.[27,39]

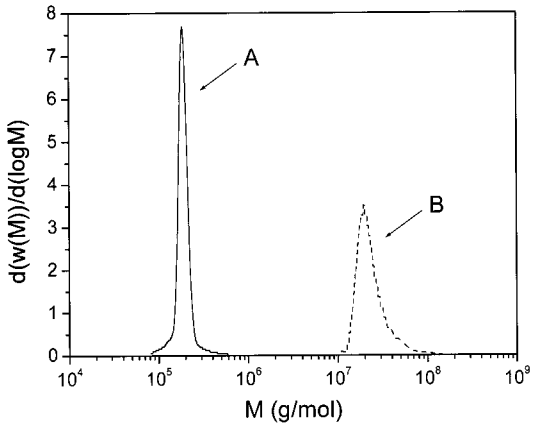

Figure 3. Molecular weight distribution of SBM (A) and SBM cross-linked with S_2Cl_2 (B), as determined by MALLS−GPC.

Each PB sphere is potentially a core of a Janus micelle which has a compartmentalized shell consisting of a PS and a PMMA hemisphere. Cross-linking of these cores in bulk forces the system to retain such a noncentrosymmetric structure even after dissolution (Figure 1). On the basis of the diameter of the PB spheres (7.7 ± 1.0 nm) from the TEM image and the PB bulk density it is possible to estimate the average number of SBM chains participating in a single PB sphere to be 13 ± 5. As a consequence a single Janus micelle consists of approximately 13 SBM chains and therefore has an expected molecular weight $M_n \approx 2.5 \times 10^6$. The minimum diameter of the Janus micelles in solution can be roughly estimated to be half the long period L of the SBM in bulk (see Figure 2): $^1/_2L = 22.9 \pm 1.6$ nm (radius $R = 11.4 \pm 0.8$ nm).

To study the properties of the Janus micelles, a bulk specimen of $S_{51}B_6M_{43}^{190}$ was cross-linked and the purified product redissolved. Films of the cross-linking product cast from $CHCl_3$ solution also show a bulk ls-morphology as the precursor SBM, thus confirming its noncentrosymmetric structure.

To determine the molecular weight, MALLS−GPC traces were recorded with THF as eluent. Using a combination of refractive index detector and MALLS detector, this method provides the true number-average molecular weight of block copolymers.[40] Figure 3 shows the differential molecular weight distributions of both precursor SBM and SBM cross-linked with S_2Cl_2. The SBM shows a very narrow molecular weight distribution ($M_{w,app}/M_n = 1.02$) with $M_n = 1.63 \times 10^5$. This M_n value is about 14% smaller than the M_n value mentioned above thus giving us an estimate of the error of these two methods. The SBM cross-linked with S_2Cl_2 shows a somewhat broader distribution ($M_{w,app}/M_n = 1.22$). The obtained $M_n = 2.08 \times 10^7$ is about 10 times higher than expected (see above).

The GPC results are confirmed by asymmetric flow field-flow fractionation in THF. Both cross-linking strategies lead to similar eluograms, thus indicating an effective cross-linking of the PB domains of the ls-morphology. However, cross-linking with AIBN also leads to some degradation of the chains. In the following, we will only discuss results on the sample cross-linked with S_2Cl_2, since there are no degradation products to be separated from the material prior to further investigations.

The large difference of the expected molecular weight of the Janus micelles and the value obtained by MALLS−

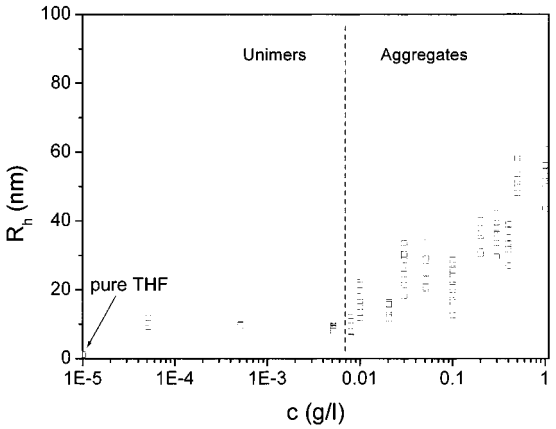

Figure 4. FCS data for the Janus micelles in THF: hydrodynamic radius of the particles carrying a dye molecule vs polymer concentration ($c = 0.515 \times 10^{-4}$ to 1 g/L). The critical aggregation concentration (cac) is taken as the concentration where the radius starts to increase (cac $\approx 7 \pm 2$ mg/L).

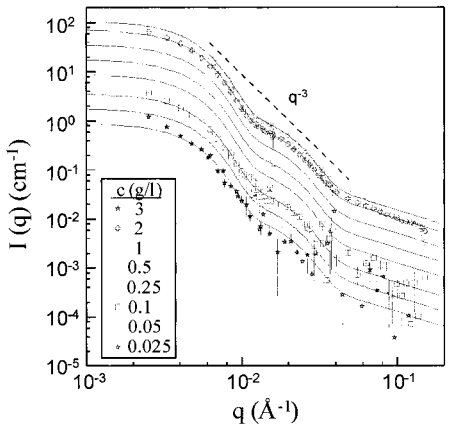

Figure 5. SANS data for the Janus micelles in THF-d_8 in a concentration range 0.025−3 g/L.

GPC was seen as a motivation to further investigate the solution behavior of the Janus micelles.

Fluorescence Correlation Spectroscopy. FCS allows to investigate the aggregation behavior of particles at very low concentrations not accessible by other analytical methods. In the present work, we studied Janus micelles dissolved in THF in a concentration range of 0.5×10^{-4} to 1 g/L. The FCS results are shown in Figure 4. Below a critical concentration of about 7 ± 2 mg/L particles of constant size are observed ($R_h \approx 10$ nm), which may be identified as molecularly dissolved Janus micelles. At higher concentrations, an increase of the hydrodynamic radius to about 53 nm is observed, indicating an aggregation of single Janus micelles into multimers, which will be referred to as "supermicelles" in the following. The critical concentration of about 7 ± 2 mg/L may therefore be taken as a critical aggregation concentration (cac) for the formation of supermicelles. The hydrodynamic radius, R_h, of the Janus micelle unimers of about 10 nm correlates well with the size estimated from TEM (see above). We note, however, that the absolute values of R_h measured by FCS comprise the approximation made for the waist radius (see Experimental Section). All hydrodynamic radii determined by FCS are number-averaged.

Small-Angle Neutron Scattering. Figure 5 shows the results of SANS measurements performed in deuterated THF (THF-d_8). The intensity drop with the scattering vector q excludes simple models of spherical aggregate-like structures which should show a q^{-4} envelope in the low to intermediate q range. Instead, a clear q^{-3} dependence is found. In a first attempt, the data were fitted by a spherical core−shell structure; however, unphysical values for both the scattering length densities and the dimensions were obtained.

Lacking further information on the inner structure of the particles, a Beaucage fit was applied to the data. The Beaucage fit is based on the assumption of a homogeneous average scattering length density. This procedure should lead to acceptable dimensions at least at low to intermediate q values. High q values, however, which probe the internal length scales of the whole particle, are most affected by this assumption. Therefore, the power law for the primary particle (see above) is probably an artifact.

Applying eq 3, we are able to fit all scattering curves with the same set of five parameters: the prefactors G, G_s, and B_s, and the structural dimensions R_g and R_s. Fitting B gave negligibly small values, therefore the respective term was omitted in order to reduce the number of variables. As a consequence, lacking a value for the power law exponent P, we are unable to infer any information on the shape of the superstructure. Likewise, we fixed the value of P_s to 1, as the fits yielded results close to this value. Regarding the range of large q values, an exponent $P_s = 1$ would indicate an extended internal structure possibly due to unfavorable interactions between PS and PMMA. However more detailed information about the structure of the particle is lacking and could only be obtained by further experiments of elaborate contrast-matching of components.

We emphasize that the presented Beaucage theory clearly indicated three regimes, corresponding to large aggregates, subunits, and a power law regime. The fit results are listed in Table 1. The first two regimes yield the sizes of the respective particles ($R_g = 35.5$ nm, $R_s = 9.9$ nm) whereas the power law term only concerns the internal structure, which is outside the scope of this publication. We note that convolution of eq 3 with the resolution function of Pedersen et al.[41,42] did not significantly change the results on R_g and R_s (see Table 1).

Table 1. SANS Fit Results from the Beaucage Model Where the Upper and Lower Rows Display, Respectively, the Results of Fits with and without Inclusion of Instrumental Resolution

G (cm^{-1})	R_g (nm)	B^a (1)	G_s (cm^{-1})	R_s (nm)	B_s (10^7)	$P_s{}^a$ (1)
34500 ± 330	**35.5 ± 0.1**	0	586 ± 15	**9.9 ± 0.1**	5.2 ± 0.2	1
35890 ± 331	**36.2 ± 0.1**	0	570 ± 15	**9.9 ± 0.1**	5.1 ± 0.2	1

[a] Kept constant.

Light Scattering. To further elucidate the solution properties of the Janus micelles, SLS experiments were performed in THF (0.025 g/L $\leq c \leq$ 3 g/L). The analysis of the scattering intensities using a Zimm plot[43] (Figure 6) yields a molecular weight $M_{w,app} = 3.45 \times 10^7$, a radius of gyration $R_{g,app} = 69$ nm and a second virial coefficient (of the osmotic pressure) $A_2 = 4.52 \times 10^{-6}$ mol·mL/g^2. These quantities are apparent quantities due to the well-known problem of static light scattering analysis of block copolymers especially in the case of PS-*block*-PMMA in THF ($\Delta dn/dc \approx 0.1$).[44,45] However, it has been shown that the chemical heterogeneity of aggregates (micelles) made from a considerable number of unimers is much smaller than the heterogeneity of the unimers and that in this case SLS yields the true

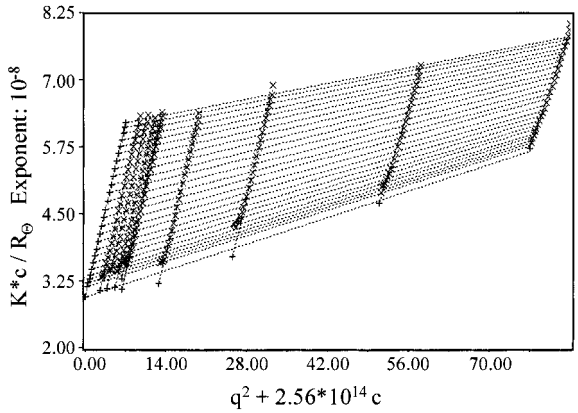

Figure 6. Zimm plot of the Janus micelles in THF in a concentration range 0.025−3 g/L.

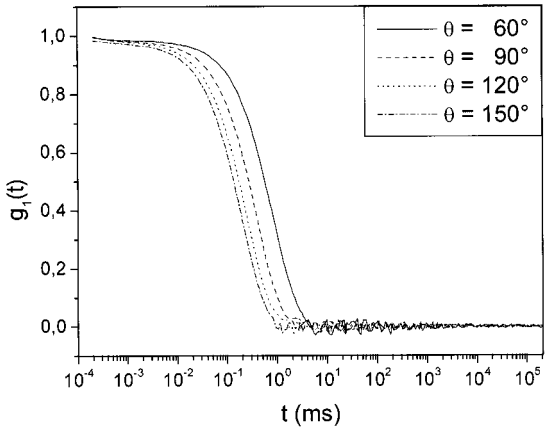

Figure 7. Field autocorrelation functions of the Janus micelles in THF at a concentration of 0.5 g/L.

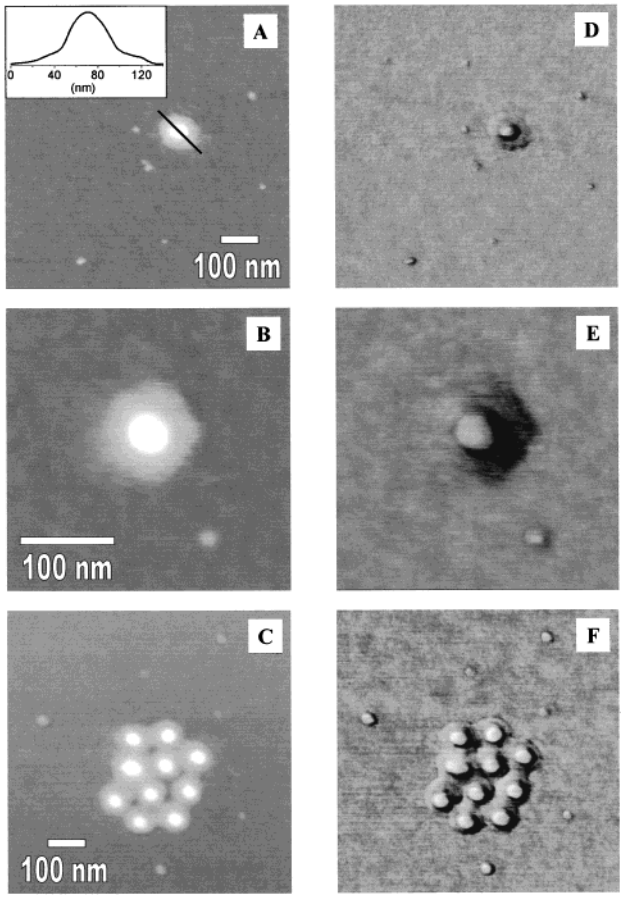

Figure 8. Tapping mode SFM images of Janus micelles and their superstructures on a silicon wafer (dip coated from a 0.01 g/L solution in THF). A−C: topography (0−30 nm). D−F: phase (D and E, 0−10°; F, 0−30°).

M_w.[46,47] Consequently the measured $M_{w,app}$ should at least be close to the true M_w, while the measured radius of gyration has to be treated as an apparent value without more detailed information about the shape of the aggregates.

It is interesting to note the linear dependence of Kc/R_θ on q^2. In the case of spherical aggregates in solution, a distinct upward curvature in the Zimm plot is expected (also for coillike structures at such high molecular weights). One may argue that the upward curvature is compensated by a downward curvature due to the polydispersity of the aggregates. However, without further supporting evidence these assumptions are purely speculative. A rodlike shape would cause a downward curvature which is also not observed. The interpretation is furthermore complicated by the fact that most of the scattering intensity is due to the PS part of the Janus micelles which has the predominant refractive index increment. The reason for the absence of the concentration dependence characteristic for aggregation phenomena in the Zimm plot[48] is that the cac (as determined by FCS) is too small to be accessible to SLS.

In addition to SLS, DLS was performed on solutions of two different concentrations (0.005 and 0.5 g/L) in THF. The CONTIN analysis[49] of the autocorrelation functions measured at four different angles (60, 90, 120, and 150°) (Figure 7) for both concentrations shows only one peak. The hydrodynamic radius of the corresponding species in solution was found to be $R_h = 74$ nm (by extrapolating $R_h(q^2)$ to $q^2 \rightarrow 0$). Because the experiments were done at concentrations $c \geq$ cac and because the hydrodynamic radius determined by light scattering is *z*-averaged,[50] only aggregates and no unimers were observed. It is obvious that the *z*-averaged hydrodynamic radius determined by DLS ($\langle R_h^{-1}\rangle_z^{-1} = 74$ nm) is larger than the number-averaged hydrodynamic radius from FCS ($\langle R_h\rangle_n = 53$ nm).

Scanning Force Microscopy. To visualize the aggregates by SFM, the micelles were deposited onto polished silicon wafers by dip coating from very dilute solutions ($c = 0.01$ g/L). Figure 8 shows tapping mode topography and phase images of micelles obtained from THF. We observe both small particles and larger structures, the latter resembling the shape of a fried egg: They exhibit an elevated middle part which is surrounded by a corona that spreads on the surface. A cross section shown as inset in Figure 8A further underlines this shape. It is difficult to infer an inner structure from the SFM images of the smaller particles; however, in some of the cases a similar "fried egg"-like morphology can be seen (see, e.g., Figure 8D,E).

If we consider the well-known preference of PMMA for polar substrates like silicon oxide[51,52] and keep in mind the Janus character of the micelles with a PS and a PMMA hemisphere, we may assume that the corona of the particles consists of the PMMA blocks whereas the elevated middle part is formed by PS. According to their sizes, the two objects in Figure 8, parts B and E, can be assigned as representative examples for the largest single aggregate (mean radius $\approx 50 \pm 10$ nm) and the smallest subunit, a unimer (mean radius $\approx 7 \pm 2$ nm).[53] These dimensions agree well with values for

supermicelles and single Janus micelles, respectively, as found in dilute solution (see above). At this point it is important to note that so far only little is known about the differences in size between the micelles in solution and deposited on a polar substrate. Swelling in solution and stretching of the polymer chains in contact with the substrate most certainly significantly influence the dimensions of the Janus particles. Although the concentration of the solutions used for the dip coating process is above the cac of 7 ± 2 mg/L, we find a remarkably large number of unimers on the wafer surface. As we also observe objects between the size of unimers and supermicelles which we do not find in solution, we may conclude that these structures are formed during the dip coating process. It is well-known that solvent evaporation can induce mechanical forces that may lead to the destruction of large aggregates formed in solution. On the other hand, the dip coating process can induce additional aggregation phenomena. After dip coating, the solution deposited onto the silicon wafer evaporates slowly and undergoes variations in concentration (from dilute to highly concentrated) before the solvent has evaporated completely. Obviously, the supermicelles already exhibit a certain critical size and therefore, instead of successively forming even larger aggregates, instead assemble on the surface to form a hexagonally packed array as shown in Figure 8, parts C and F. In summary, the Janus micelles were found to organize on different levels on the substrate surface: single micelles (unimers), supermicelles, and their hexagonal arrays.

Comparison of Results Obtained by Different Techniques and Conclusion. FCS experiments give an overview of the Janus micelles' association behavior in THF and provide a critical aggregation concentration cac $\approx 7 \pm 2$ mg/L and approximate hydrodynamic radii of both unimer ($\langle R_h \rangle_n \approx 10$ nm) and supermicelles ($\langle R_h \rangle_n \approx 53$ nm). SANS confirms the existence of aggregates in a concentration range above the cac. A Beaucage fit of the scattering curves provides a R_g of the aggregates of 35.5 nm and a radius R_s of the substructures of 9.9 nm. Dynamic light scattering gives a hydrodynamic radius $\langle R_h^{-1} \rangle_z^{-1} = 74$ nm of the supermicelles.

Using the true M_n values determined by MALLS−GPC of the precursor SBM and the supermicelles and the number of SBM chains in one Janus micelle from TEM (see Synthesis) and further taking into account the increase of mass per SBM chain by addition of sulfur and chlorine during the cross-linking reaction, it is possible to calculate an approximate aggregation number of 11 ± 4. The Janus micelles also exhibit a bulk ls-morphology as the precursor SBM polymer confirming their noncentrosymmetric structure. However, so far there is no experimental evidence regarding the shape of the supermicelles in solution. Further SANS experiments with contrast-matching are necessary in order to clarify this issue.

SFM allows to visualize both unimers and aggregates precipitated on a silicon oxide surface and confirms the amphiphilic nature (surface acitivity) of the Janus micelles.

What has not been discussed so far is the important question why these Janus micelles show aggregation into supermicelles at all, because THF supposedly is a good solvent for both PS and PMMA. One may argue that the slight differences in solubility of individual PS and PMMA chains are amplified by bundling up several block copolymer chains into a Janus micelle. Slightly different degrees of swelling might induce a curvature of the PS/PMMA interface which may in turn lead to aggregation. Another suggestion is that chains in both hemispheres experience a loss in conformational entropy due to the cross-linking which can be diminished by forming larger phases (aggregates). However, the issue of supermicelle formation in THF is still open and further discussion is needed.

In summary, we have demonstrated a synthetic route for the formation of compartmentalized micellar objects by suitably preserving the molecular superstructure of a microphase separated ABC triblock copolymer (by cross-linking in the bulk phase and subsequent dissolution). Given the rich variety of morphologies known for this class of materials, this approach may well be utilized to create other complex supramolecular objects via the synthetic detour through the bulk phase.

Acknowledgment. Reimund Stadler originated this project and supervised its progress for $1^1/_2$ years. The authors are very grateful for his significant contribution to this work, the continuation of which he unfortunately did not live to see. The authors appreciate fruitful discussions with Werner Köhler, Mark Geoghegan, and Chun Wang (Bayreuth, Germany), Gernot Baur (SLS−Systemtechnik, Hausen i. W., Germany), Stephan Förster (Hamburg, Germany), Manfred Schmidt (Mainz, Germany), Igor Erukhimovich (Moscow), Sergei Sheiko and Martin Möller (Ulm, Germany). Also the help of Astrid Göpfert (Bayreuth, Germany) for TEM, Beate Müller (Mainz, Germany) for dynamic light scattering, Thorsten Klein (Postnova Analytics, München, Germany) for FFFF and Thorsten Hofe (PSS, Mainz, Germany) for MALLS−GPC and helpful discussions is highly acknowledged. A.B. acknowledges a Kekulé fellowship by Stiftung Stipendien-Fonds des Verbandes der Chemischen Industrie and BMBF. Financial support of this work was given by the Deutsche Forschungsgemeinschaft within the "Schwerpunkt Polyelektrolyte" (STA 272/8−2, MU 896/11−3) and the Bayreuther Institut für Makromolekülforschung (BIMF).

References and Notes

(1) Fredrickson, G. H.; Bates, F. S. *Annu. Rev. Mater. Sci.* **1996**, *26*, 501.
(2) Bates, F. S.; Fredrickson, G. H. *Phys. Today* **1999**, *52*, 33.
(3) Chen, Z.-R.; Issaian, A. M.; Kornfield, J. A.; Smith, S. D.; Grothaus, J. T.; Satkowski, M. M. *Macromolecules* **1997**, *30*, 7096.
(4) Matsushita, Y.; Yamada, K.; Hattori, T.; Fujimoto, T.; Sawada, Y.; Nasagawa, M.; Matsui, C. *Macromolecules* **1983**, *16*, 10.
(5) Stadler, R.; Auschra, C.; Beckmann, J.; Krappe, U.; Voigt-Martin, I.; Leibler, L. *Macromolecules* **1995**, *28*, 3080.
(6) Abetz, V. In *Supramolecular Polymers*; Ciferri, A., Ed.; Marcel Dekker Inc.: New York, 2000, p 215.
(7) Hückstädt, H.; Göpfert, A.; Abetz, V. *Polymer* **2000**, *41*, 9089.
(8) Okamoto, S.; Hasegawa, H.; Hashimoto, T.; Fujimoto, T.; Zhang, H.; Kazama, T.; Takano, A.; Isono, Y. *Polymer* **1997**, *38*, 5275.
(9) Hadjichristidis, N. *J. Polym. Sci., Part A: Polym. Chem.* **1999**, *37*, 857.
(10) Hückstädt, H.; Göpfert, A.; Abetz, V. *Macromol. Chem. Phys.* **2000**, *201*, 296.
(11) Hückstädt, H.; Goldacker, T.; Göpfert, A.; Abetz, V. *Macromolecules* **2000**, *33*, 3757.
(12) Bayer, U.; Stadler, R. *Macromol. Chem. Phys.* **1994**, *195*, 2709.
(13) Alexandridis, P.; Olsson, U.; Lindman, B. *Langmuir* **1997**, *13*, 23.
(14) Förster, S.; Antonietti, M. *Adv. Mater.* **1998**, *10*, 195.

(15) Yu, K.; Eisenberg, A. *Macromolecules* **1998**, *31*, 3509.
(16) Voulgaris, D.; Tsitsilianis, C.; Grayer, V.; Esselink, F. J.; Hadziioannou, G. *Polymer* **1999**, *40*, 5879.
(17) Giebeler, E.; Stadler, R. *Macromol. Chem. Phys.* **1997**, *198*, 1385.
(18) Yu, G.; Eisenberg, A. *Macromolecules* **1998**, *31*, 5546.
(19) Stewart, S.; Liu, G. *Chem. Mater.* **1999**, *11*, 1048.
(20) Bieringer, R.; Abetz, V.; Müller, A. H. E. *Eur. Phys. J. E*, submitted for publication.
(21) Liu, G.; Quiao, L.; Guo, A. *Macromolecules* **1996**, *29*, 5508.
(22) Casagrande, C.; Veyssié, M. *C. R. Acad. Sci. (Paris) II* **1988**, *306*, 1423.
(23) Casagrande, C.; Fabre, P.; Raphaël, E.; Veyssié, M. *Europhys. Lett.* **1989**, *9*, 251.
(24) Bo, Z.; Rabe, J. P.; Schlüter, A. *Angew. Chem.* **1999**, *111*, 2540.
(25) Heroguez, V.; Gnanou, Y.; Fontanille, M. *Macromolecules* **1997**, *307*, 4791.
(26) Goldacker, T.; Abetz, V.; Stadler, R.; Erukhimovich, I.; Leibler, L. *Nature* **1999**, *398*, 137.
(27) Abetz, V.; Goldacker, T. *Macromol. Rapid Commun.* **2000**, *21*, 16.
(28) Auschra, C.; Stadler, R. *Polym. Bull. (Berlin)* **1993**, *30*, 257.
(29) Ohnuma, H.; Shimohira, T.; Tanisugi, H.; Kudose, I.; Kotaka, T. *Bull. Inst. Chem. Res., Kyoto Univ.* **1988**, *66*, 283.
(30) Ishizu, K.; Onen, A. *J. Polym. Sci., Part A*: *Polym. Chem.* **1989**, *27*, 3721.
(31) Glazer, J. *J. Polym. Sci.* **1954**, *14*, 225.
(32) Giddings, J. C. *Science* **1993**, *260*, 1456.
(33) Ratanathanawongs, S. K.; Giddings, J. C. *ACS Symp. Ser.* **1993**, *521*, 13.
(34) Elson, E. L.; Magde, D. *Biopolymers* **1974**, *13*, 1.
(35) Rigler, R.; Widengren, J.; Mets, Ü. In *Fluorescence Spectroscopy*; Wolfbeis, O. S., Ed.; Springer-Verlag: Berlin, 1993; p 13.
(36) Beaucage, G. *J. Appl. Crystallogr.* **1995**, *28*, 717.
(37) Becker, A.; Köhler, W.; Müller, B. *Ber. Bunsen-Ges. Phys. Chem.* **1995**, *99*, 600.
(38) A sample of PS taken from the polymerization solution before the addition of the second monomer, butadiene.
(39) Breiner, U.; Krappe, U.; Thomas, E. L.; Stadler, R. *Macromolecules* **1998**, *31*, 135.
(40) Radke, W.; Simon, P. F.; Müller, A. H. E. *Macromolecules* **1996**, *29*, 4926.
(41) Pedersen, J. S.; Posselt, D.; Mortensen, K. *J. Appl. Crystallogr.* **1990**, *23*, 321.
(42) Pedersen, J. S. *J. Phys. IV* **1993**, *3*, 491.
(43) Zimm, B. H. *J. Chem. Phys.* **1948**, *16*, 1099.
(44) Benoit, H.; Froehlich, D. In *Light Scattering from Polymer Solutions*; Huglin, M. B., Ed.; Academic Press: London, 1972; p 467.
(45) Kratochvil, P. In *Classical Light Scattering from Polymer Solutions*; Jenkins, A. D., Ed.; Elsevier: Amsterdam, 1987; p 187.
(46) Vorlicek, J.; Kratochvil, P. *J. Polym. Sci., Polym. Phys. Ed.* **1973**, *11*, 1251.
(47) Quin, A.; Tian, M.; Ramireddy, C.; Webber, S. E.; Munk, P.; Tuzar, Z. *Macromolecules* **1994**, *27*, 120.
(48) Elias, H. G. In *Light Scattering from Polymer Solutions*; Huglin, M. B., Ed.; Academic Press: London, 1972; p 397.
(49) Provencher, S. W. *Comput. Phys. Commun.* **1982**, *27*, 229.
(50) To be more precise DLS provides the *z*-average of 1/hydrodynamic radius ($\langle R_h^{-1} \rangle_z$).
(51) Satija, K. S.; Majkrzak, C. F.; Russell, T. P.; Sinha, S. K.; Sirota, E. B.; Hughes, G. J. *Macromolecules* **1990**, *23*, 3860.
(52) Morkved, T. L.; Jaeger, H. M. *Europhys. Lett.* **1997**, *40*, 643.
(53) Numbers have been evaluated by measuring at least 20 unimers and supermicelles.

MA000670P